

# Acoustic Vector-Sensor Beamforming and Capon Direction Estimation

Malcolm Hawkes, *Student Member, IEEE*, and Arye Nehorai, *Fellow, IEEE*

**Abstract**— We examine the improvement attained by using acoustic vector sensors for direction-of-arrival (DOA) estimation, instead of traditional pressure sensors, via optimal performance bounds and particular estimators. By examining the Cramér–Rao bound in the case of a single source, we show that a vector-sensor array’s smaller estimation error is a result of two distinct phenomena: 1) an effective increase in signal-to-noise ratio due to a greater number of measurements of phase delays between sensors and 2) direct measurement of the DOA information contained in the structure of the velocity field due to the vector sensors’ directional sensitivity. Separate analysis of these two phenomena allows us to determine the array size, array shape, and SNR conditions under which the use of a vector-sensor array is most advantageous and to quantify that advantage. By extending the beamforming and Capon direction estimators to vector sensors, we find that the vector sensors’ directional sensitivity removes all bearing ambiguities. In particular, even simple structures such as linear arrays can determine both azimuth and elevation, and spatially undersampled regularly spaced arrays may be employed to increase aperture and, hence, performance. Large sample approximations to the mean-square error matrices of the estimators are derived and their validity is assessed by Monte Carlo simulation.

## I. INTRODUCTION

THE PASSIVE direction-of-arrival (DOA) estimation problem, in which the bearings of a number of far-field acoustic sources are determined, is of great importance in many underwater applications. The traditional solution is to use a spatially distributed array of pressure sensors, and many estimation techniques have evolved for this scenario. As demand for smaller arrays that perform better at a lower signal-to-noise ratio (SNR) has increased, the idea of measuring particle velocity, as well as pressure, has arisen [1], [2]. This has coincided with a surge of interest in particle velocity sensors and improvements in fabrication techniques [3] to make vector-sensor arrays a practical reality [4].

An acoustic vector sensor measures the acoustic pressure and all three components of the acoustic particle velocity at a single point in space. Thus, whereas standard pressure

sensors can only utilize the directional information present in the propagation delays between sensors, each vector sensor can extract further directional information directly from the structure of the velocity field. This directional information permits, for example, a single vector-sensor to identify up to two sources [5]. By making use of this extra information, arrays of vector sensors are able to improve source localization accuracy without increasing array aperture.

Both theoretical and practical work has been published on the topic of acoustic vector sensors. A model for acoustic vector sensors, a general expression for the Cramér–Rao bound (CRB), and a simple DOA estimation algorithm for a single sensor were introduced in [1] and [2]; preliminary theoretical performance analyses appear in [1], [2], [6], and [7]. In addition, ESPRIT and Root-MUSIC algorithms have recently been applied to arrays of velocity-sensor triads [8]–[10]. Meanwhile, acoustic vector sensors have been constructed [11] and linear arrays of them built and subjected to sea trials, [4], [12]–[14].

In this paper (see also [6] and [7]), we investigate and quantify the factors that lead to the improved DOA estimation performance of a vector-sensor array over a pressure-sensor array. By examining optimum performance (via the CRB) in detail for a single source, we are able to discern two distinct factors: 1) an effective increase in SNR due to extra measurements of the phase delays between noncoincident sensors and 2) a further reduction in the bound due to direct measurement of the structure of the velocity field by each vector sensor. Separate consideration of the two phenomena shows that the increase in estimation accuracy obtained by using vector sensors is greatest for linear or planar arrays [as opposed to three-dimensional (3-D) geometries], small numbers of sensors, and low SNR’s.

We then consider the conventional beamforming and Capon [15] (which is also known as minimum-variance distortionless response beamforming) direction estimators. We show that *any* vector-sensor array and, hence, the popular linear array can be used to unambiguously determine both the azimuth and elevation. This has significant practical value: For example, when using a linear towed array of vector sensors to determine the location of surface ships, the left/right ambiguity problem does not arise, avoiding the need to rotate the vessel through 90° between readings. Furthermore, we show that a vector-sensor array suffers less from spatial aliasing in an undersampled wavefield. In particular, grating lobes do not appear in the beampattern. This allows the use of undersampled regular arrays in order to extend the spatial aperture and, hence,

Manuscript received December 2, 1996; revised December 19, 1997. This work was supported by the Air Force Office of Scientific Research under Grant F49620-97-1-0481, the National Science Foundation under Grant MIP-9615590, and the Office of Naval Research under Grant N00014-96-1-1078. The associate editor coordinating the review of this paper and approving it for publication was Prof. Victor A. N. Barroso.

M. Hawkes is with the Department of Electrical Engineering and Computer Science, University of Illinois, Chicago, IL 60607 USA, on leave from the Department of Electrical Engineering, Yale University, New Haven, CT 06520 USA.

A. Nehorai is with the Department of Electrical Engineering and Computer Science, University of Illinois, Chicago, IL 60607 USA.

Publisher Item Identifier S 1053-587X(98)05953-4.

improve estimation performance. We also derive large sample approximations to the mean-square error of both estimators for the vector-sensor array. These approximations are validated with Monte Carlo simulations.

In Section II, we state the mathematical model for the measurements of a vector-sensor array. In Section III, we analyze the CRB for a single source in some depth. In Section IV, we consider the beamforming and Capon estimators and derive the large sample MSE approximations. In Section V, we give some numerical examples and conclude the paper in Section VI.

## II. MEASUREMENT MODEL

We consider  $n$  narrowband planewaves, with common center frequency  $\omega$ , traveling in an isotropic, quiescent, homogeneous fluid medium and impinging on an array of  $m$  acoustic vector sensors (see [2] for details). Each planewave is parameterized by its azimuth  $\phi \in (0, 2\pi]$  and elevation  $\psi \in [-\pi/2, \pi/2]$ , and the problem is to determine the DOA parameter vector  $\boldsymbol{\theta} = [\boldsymbol{\theta}_1^T, \dots, \boldsymbol{\theta}_n^T]^T$ , where  $\boldsymbol{\theta}_k = [\phi_k, \psi_k]^T$  is the DOA of the  $k$ th source.

### A. Array Output

Acoustic pressure and particle velocity are related by Euler's equation [16], which is

$$\mathbf{v}(\mathbf{r}, t) = -\frac{p(\mathbf{r}, t)}{\rho_0 c} \mathbf{u} \quad (1)$$

for a planewave, where  $\mathbf{v}(\mathbf{r}, t)$  and  $p(\mathbf{r}, t)$  denote the (vector) acoustic particle velocity and (scalar) acoustic pressure at position  $\mathbf{r}$  and time  $t$ ,  $\rho_0$  is the ambient pressure,  $c$  is the speed of sound in the medium, and  $\mathbf{u} = [\cos \phi \cos \psi, \sin \phi \cos \psi, \sin \psi]^T$  is the source's bearing vector (i.e., the unit length vector pointing from the origin toward the source).

Practical acoustic vector sensors consist of a co-located pressure sensor (hydrophone) and triad of orthogonal velocity sensors (geophones) [4] and [11]. We assume that the output of each geophone is proportional to the cosine of the angle between  $\mathbf{u}$  and one of the coordinate axes. This assumption requires that 1) the geophones have a cosine response and 2) each of the  $m$  vector sensors in the array has a known orientation and that this orientation is used to rotate the data to align them with the coordinate axes.

Using complex-envelope (phasor) representation, it follows from (1) that the output of a vector sensor, which is located at  $\mathbf{r}$ , is a four-element complex vector

$$\begin{bmatrix} y_p(t) \\ \mathbf{y}_v(t) \end{bmatrix} = \sum_{k=1}^n \begin{bmatrix} 1 \\ \mathbf{u}_k \end{bmatrix} e^{-i\omega\tau_k} p_k(t) + \begin{bmatrix} e_p(t) \\ \mathbf{e}_v(t) \end{bmatrix} \quad (2)$$

where  $y_p(t)$  and  $\mathbf{y}_v(t)$  are the outputs of the pressure sensor and velocity sensors, respectively,  $p_k(t)$  is the pressure complex envelope of the  $k$ th wave at the origin, and  $e_p(t)$  and  $\mathbf{e}_v(t)$  represent noise. The variable  $\tau_k$  is the differential time delay of the  $k$ th wave between the origin and the sensor and is given by  $\tau_k = -(\mathbf{r}^T \mathbf{u}_k)/c$ . Note that in (2), we have normalized

the velocity measurements by multiplying by  $-\rho_0 c$ , which is assumed to be known.

The output of an array, with vector sensors located at  $\mathbf{r}_1, \dots, \mathbf{r}_m$ , is a single  $4m$  vector obtained by stacking the  $m$  four-element measurement vectors. It may be written using the array processing equation

$$\mathbf{y}(t) = A(\boldsymbol{\theta})\mathbf{p}(t) + \mathbf{e}(t) \quad (3)$$

where  $A(\boldsymbol{\theta}) = [\mathbf{a}(\boldsymbol{\theta}_1), \dots, \mathbf{a}(\boldsymbol{\theta}_n)]$ , and  $\mathbf{p}(t)$  contains the  $n$  source signals. The difference between (3) and the usual omnidirectional sensor model is in the steering vector  $\mathbf{a}(\boldsymbol{\theta}_k)$ , which is the array's response to a unit amplitude planewave from direction  $\boldsymbol{\theta}_k$ . It follows from (2) that  $\mathbf{a}(\boldsymbol{\theta}_k)$  is given by the Kronecker product

$$\mathbf{a}(\boldsymbol{\theta}_k) = \mathbf{a}_P(\boldsymbol{\theta}_k) \otimes \mathbf{h}(\boldsymbol{\theta}_k) \quad (4)$$

where

$$\mathbf{a}_P(\boldsymbol{\theta}_k) = [e^{i2\pi(\mathbf{r}_1^T \mathbf{u}_k)}, \dots, e^{i2\pi(\mathbf{r}_m^T \mathbf{u}_k)}]^T \quad (5)$$

$$\mathbf{h}(\boldsymbol{\theta}_k) = [1, \mathbf{u}_k^T]^T \quad (6)$$

and  $\mathbf{r}_1, \dots, \mathbf{r}_m$  are in units of wavelengths. Note that  $\mathbf{a}_P(\boldsymbol{\theta}_k)$  is the steering vector of an equivalent pressure sensor array, i.e., an array with a single pressure sensor at each location  $\mathbf{r}_1, \dots, \mathbf{r}_m$ , whereas  $\mathbf{h}(\boldsymbol{\theta}_k)$  is the response of a single vector sensor located at the origin. The vector  $\mathbf{a}_P(\boldsymbol{\theta}_k)$  contains the phase delay information between noncoincident sensors and depends only on the sensor locations. On the other hand,  $\mathbf{h}(\boldsymbol{\theta}_k)$  accounts for the directional response of each component—omnidirectional for the pressure sensor and cosine for the velocity sensors—and is *independent* of the position of each sensor. It therefore conveys the DOA information present in the structure of the velocity field. It is the assumption that all vector sensors have a common alignment with the coordinate axes (by a rotation of the data) that permits the above Kronecker product expression for the steering vector. This, in turn, will allow us to obtain CRB expressions in which the distinct effects of sensor location and inherent directional sensitivity may be separately analyzed. Note that the usual pressure-sensor array model is a special case of this model obtained by setting  $\mathbf{h}(\boldsymbol{\theta}_k) = 1$ .

### B. Statistical Assumptions

We assume that both the signal  $\mathbf{p}(t)$  and the noise  $\mathbf{e}(t)$  are independent identically distributed (i.i.d.), zero-mean, complex Gaussian processes. In addition, we assume that  $\mathbf{p}(t)$  and  $\mathbf{e}(s)$  are independent for all  $s$  and  $t$ . These two processes are completely characterized by their covariance matrices

$$E\{\mathbf{p}(t)\mathbf{p}^H(t)\} = P \quad (7)$$

$$E\{\mathbf{e}(t)\mathbf{e}^H(t)\} = I_m \otimes \begin{bmatrix} \sigma_p^2 & 0 \\ 0 & \sigma_v^2 I_3 \end{bmatrix} \quad (8)$$

where the superscript  $H$  represents conjugate transposition,  $\sigma_p^2$  and  $\sigma_v^2$  are the pressure-sensor and velocity-sensor noise variances, respectively, and  $I_m$  is the  $m$ th-order identity matrix. The assumed structure of the noise covariance is consistent with internal sensor noise. We allow the noise power

to differ between pressure and velocity sensors to account for their different construction and the latter's directional sensitivity. With these assumptions, the data is also an i.i.d., zero-mean, complex Gaussian process with covariance matrix

$$R = A(\boldsymbol{\theta})PA^H(\boldsymbol{\theta}) + I_m \otimes \begin{bmatrix} \sigma_p^2 & 0 \\ 0 & \sigma_v^2 I_3 \end{bmatrix}. \quad (9)$$

The unknowns are the  $2n$  DOA parameters  $\boldsymbol{\theta}$ , the signal covariance  $P$ , and the noise variances  $\sigma_p^2$  and  $\sigma_v^2$ . Thus, the unknown parameter vector is  $\boldsymbol{\gamma} = [\boldsymbol{\theta}^T, \vec{P}^T, \sigma_p^2, \sigma_v^2]^T$ , where  $\vec{P}^T$  is a vector containing  $n^2$  free real parameters of the Hermitian matrix  $P$ , giving a total of  $n^2 + 2n + 2$  real unknowns.

### III. OPTIMUM PERFORMANCE

In this section, we analyze the CRB on the DOA parameters in the case of a single source. By comparing the bound for a vector-sensor array with that for a traditional pressure-sensor array, we quantify two distinct factors that contribute to the former's improved performance: an effective increase in SNR due to a greater number of measurements of the intersensor phase delays and direct measurement of the DOA information contained in the structure of the velocity field by virtue of the vector sensors' inherent directional sensitivity. We then determine conditions under which the use of vector sensors is most advantageous.

Theorem 3.1 of [2] gives a compact matrix expression for the CRB on the DOA parameters  $\boldsymbol{\theta}$  with an acoustic vector-sensor array. This result only requires inversion of a  $2n \times 2n$  matrix, where  $n$  is the number of sources, instead of the full Fisher information matrix (FIM). Using this theorem, the CRB on azimuth and elevation, in the case of a single source, is (see [17] or [18] for the derivation)

$$\text{CRB}_P(\boldsymbol{\theta}) = \frac{1}{2N} \frac{1}{m\rho} \left(1 + \frac{1}{m\rho}\right) J^{-1} \quad (10)$$

$$\text{CRB}_V(\boldsymbol{\theta}) = \frac{1}{2N} \frac{1}{m\rho\rho_I} \left(1 + \frac{1}{m\rho\rho_I}\right) [J + K]^{-1} \quad (11)$$

where (10) is the pressure-sensor and (11) the vector-sensor expression,  $\rho = P/\sigma_p^2$  is the SNR at each pressure sensor,  $\rho_I = (1 + 1/\eta)$  is the effective increase in SNR (see below), and  $\eta = \sigma_v^2/\sigma_p^2$  is the ratio of noise powers for the two types of sensor. When the origin of the coordinate system is the array centroid,  $J$  and  $K$  are given by

$$J = \frac{4\pi^2}{m} \begin{bmatrix} \cos^2 \psi \sum (\mathbf{r}_j^T \mathbf{v}_\phi)^2 & \cos \psi \sum \mathbf{r}_j^T \mathbf{v}_\phi \mathbf{r}_j^T \mathbf{v}_\psi \\ \cos \psi \sum \mathbf{r}_j^T \mathbf{v}_\phi \mathbf{r}_j^T \mathbf{v}_\psi & \sum (\mathbf{r}_j^T \mathbf{v}_\psi)^2 \end{bmatrix}$$

$$K = \frac{1}{1 + \eta} \begin{bmatrix} \cos^2 \psi & 0 \\ 0 & 1 \end{bmatrix}$$

where  $\mathbf{v}_\phi = (\partial \mathbf{u} / \partial \phi) / \cos \psi$ ,  $\mathbf{v}_\psi = \partial \mathbf{u} / \partial \psi$ ,  $\mathbf{r}_1, \dots, \mathbf{r}_m$  are in units of wavelengths, and the sums are over the number of sensors  $m$ . Note that in (10) and (11), we have only to invert symmetric  $2 \times 2$  matrices, even though there are five unknowns. In [17] and [18], we show that the vector-sensor array's  $5 \times 5$  FIM is block diagonal for this single source scenario. Thus,

$\text{CRB}_V(\boldsymbol{\theta})$  is independent of whether  $\sigma_p^2$ ,  $\sigma_v^2$ , and  $P$  are known or not and is just the inverse of the appropriate principal submatrix of the FIM.

The vector-sensor expression differs from the pressure-sensor expression in two ways: It contains extra factors of  $(1 + 1/\eta)$  and an extra additive term  $K$ , both of which reduce  $\text{CRB}_V(\boldsymbol{\theta})$  relative to  $\text{CRB}_P(\boldsymbol{\theta})$ . The former represents an effective increase in SNR due to the greater number of measurements made by the vector-sensor array, whereas the latter results from direct measurement of the DOA information contained in the structure of the velocity field by each vector sensor's inherent directional sensitivity.

It may at first seem unfair to compare the vector-sensor array and pressure-sensor array because the former makes four times as many measurements as the latter. It may seem that a fairer comparison would be "equal aperture, equal measurements," i.e., an array of  $4m$  pressure sensors occupying the same aperture as an array of  $m$  vector sensors, and indeed, such a comparison is made numerically in Section V. However, in a practical system, a considerable portion of the cost is related to the construction, deployment, and location calibration of sensor packages. Since these arrays contain the same number of sensor packages, they have similar costs in these areas; therefore, it is not at all obvious that this comparison is any fairer. Furthermore, the detailed analytical comparison that we are able to provide here is facilitated by the relationship between the two arrays' steering vectors (4). This relationship would be lost in an equal aperture, equal measurements comparison, reducing us to numerical comparisons of particular array structures that would not reveal the more general conclusions we obtain.

#### A. SNR Increase

Denote by  $\text{CRB}_{\text{SNR}}(\boldsymbol{\theta})$  the vector-sensor bound ignoring the directional sensitivity, i.e., expression (11) with  $K = 0$ . Then, from (10) and (11), the difference between  $\text{CRB}_P(\boldsymbol{\theta})$  and  $\text{CRB}_{\text{SNR}}(\boldsymbol{\theta})$  is simply an increase in SNR from  $\rho$  to  $\rho\rho_I$ . By ignoring  $K$ , we are using only the phase delay information between sensors; the increase in SNR is due to the vector-sensor array's extra measurements of the *same set* of phase delays made by the pressure-sensor array. The factor of increase  $\rho_I = 1 + 1/\eta$  arises as follows. First, note that  $\eta$  may be written as  $\eta = (P/\sigma_p^2)/(P/\sigma_v^2)$ , i.e., the ratio of the SNR at each pressure sensor to the nominal SNR at each velocity sensor. The SNR at a pressure sensor is independent of the DOA; however, the true SNR at a velocity sensor is proportional to the square of the cosine of the angle between the source bearing and its axis, only achieving the nominal SNR of  $P/\sigma_v^2$  when the wave is parallel to its axis. A velocity-sensor triad has output proportional to the unit vector  $\mathbf{u}$  and, thus, a combined SNR of  $P|\mathbf{u}|^2/\sigma_v^2 = P/\sigma_v^2$ , which is independent of the DOA. Together, the velocity triad and pressure sensor have a combined SNR of  $P/\sigma_p^2 + P/\sigma_v^2 = \rho\rho_I$ .

The value of  $\eta$  critically effects the usefulness of the vector-sensor array; for small  $\eta$ , the SNR increase  $\rho_I$  is very large but it is negligible for large  $\eta$ . If all the noise is internal sensor noise, then  $\eta$  is a direct reflection of the relative

noise floors of the two types of sensor, and the technology is available to make them approximately equal [3], i.e.,  $\eta = 1$ . If ambient noise is present, then  $\eta < 1$  since the velocity sensors filter out some of the unwanted noise, for example,  $\eta = 1/3$  for spherically isotropic noise (this can be derived from the results of [19]); however, our assumption of spatial whiteness (8) is not generally valid for ambient noise. In one experiment [20], it was observed that if water flow past the sensors is fast enough to become turbulent on the surface of the sensor packaging, then the velocity sensor measurements were more adversely affected than those of the pressure sensors, leading to  $\eta > 1$ . However, it has been shown that flow noise can be significantly reduced by encasing the sensors in elastomer [21]; this was not done in [20]. Therefore, although the usefulness of stationary or slowly drifting vector sensors has been demonstrated at sea [11], [12], and [14], more experimental work needs to be done to determine the practicality of vector sensors in towed deployment.

Continuing to ignore the directional term  $K$ , we assess the effect of the SNR increase on the CRB. Let  $r_{\text{SNR}}$  denote the ratio of the entries of  $\text{CRB}_{\text{SNR}}(\boldsymbol{\theta})$  [i.e.,  $\text{CRB}_V(\boldsymbol{\theta})$  with  $K = 0$ ] to the entries of  $\text{CRB}_P(\boldsymbol{\theta})$ . Then

$$r_{\text{SNR}} = \rho_I^{-1} \left( \frac{m\rho + \rho_I^{-1}}{m\rho + 1} \right) \quad (12)$$

which depends only on the product of the number of sensors and the SNR  $m\rho$  and the SNR increase  $\rho_I$ . Clearly, the smaller  $r_{\text{SNR}}$ , the smaller  $\text{CRB}_{\text{SNR}}(\boldsymbol{\theta})$  relative to  $\text{CRB}_P(\boldsymbol{\theta})$  and, hence, the greater the performance gain produced by the SNR increase. Since  $\rho_I > 1$ , it follows that if  $m\rho \ll 1/\rho_I$ , then  $r_{\text{SNR}} \approx \rho_I^{-2}$ , but if  $m\rho \gg 1$ , then  $r_{\text{SNR}} \approx \rho_I^{-1}$ . Thus, for a given  $\eta$  (and, hence,  $\rho_I$ ),  $r_{\text{SNR}} \in (\rho_I^{-2}, \rho_I^{-1})$ , toward the lower end of the range when  $m\rho$  is small and toward the upper end when  $m\rho$  is large. Thus, in terms of the effective increase in SNR, the vector-sensor array is most advantageous when  $m\rho$  is small, i.e., for small numbers of sensors and low SNR's; the particular array geometry is irrelevant. Naturally, for any value of  $m\rho$ ,  $r_{\text{SNR}}$  decreases as  $\eta$  decreases (and, hence,  $\rho_I$  increases), leading to improved vector-sensor array performance.

### B. Directional Sensitivity

The output of each velocity sensor triad is proportional to the bearing  $\mathbf{u}$  [see (2)]. Thus, the measurement of each vector sensor contains additional directional information that unlike the phase delay information, is quite independent of any other sensor. This information, which results in the existence of the matrix  $K$  in the bound, further reduces the vector-sensor CRB relative to the pressure-sensor bound. In contrast to  $J$ , which represents the phase delay information,  $K$  is independent of the array geometry and DOA (the  $\cos^2 \psi$  term in the expression for  $K$  is merely a consequence of the singularity of the spherical coordinate system and may be ignored). Furthermore, it is diagonal, i.e., the information on azimuth is independent of the information on elevation and vice versa, it is always nonsingular, and ignoring the  $\cos^2 \psi$  term, the diagonal entries are equal. Thus, any array

of vector sensors provides information about both the azimuth and elevation, and the directional sensitivity provides the same amount of information about each DOA parameter.

From (11) and the expressions for  $J$  and  $K$ , the directional information makes a significant reduction in the bound if either of

$$J_{\phi\phi} \triangleq \sum_j (\mathbf{r}_j^T \mathbf{v}_\phi)^2 \gg \frac{m}{4\pi^2(1+\eta)} \quad (13)$$

$$J_{\psi\psi} \triangleq \sum_j (\mathbf{r}_j^T \mathbf{v}_\psi)^2 \gg \frac{m}{4\pi^2(1+\eta)} \quad (14)$$

hold. The effect is on azimuth if (13) holds and elevation if (14) holds. Examination of (13) and (14) shows that  $J_{\phi\phi}$  and  $J_{\psi\psi}$  are in fact the sum of squares of the projections of the position vectors onto  $\mathbf{v}_\phi$  and  $\mathbf{v}_\psi$ , respectively; hence, we term them squared projected apertures. Now,  $\mathbf{u}$ ,  $\mathbf{v}_\phi$ , and  $\mathbf{v}_\psi$  are mutually orthogonal, with  $\mathbf{u}$  pointing toward the source and  $\mathbf{v}_\phi$  lying in the  $x, y$  plane. Therefore,  $J_{\phi\phi}$  and  $J_{\psi\psi}$  are the squared projected apertures onto two orthogonal directions that are also perpendicular to the bearing  $\mathbf{u}$ . We may think of them as the total squared aperture(s) "seen" by the source:  $J_{\phi\phi}$  as the total squared aperture "seen" in the  $x, y$  plane and  $J_{\psi\psi}$  as that seen orthogonal to  $\mathbf{v}_\phi$ . The directional sensitivity plays an important role whenever either one of the squared projected apertures is not too large relative to  $m/(4\pi(1+\eta))$ . First, note that the smaller  $\eta$  is, the greater the directional sensitivity's effect. Second, since  $J_{\phi\phi}$  and  $J_{\psi\psi}$  depend on the DOA and array geometry, so does the *relative* contribution of the directional sensitivity to the total Fisher information. Finally, for linear and planar arrays,  $K$  will always be significant for some particular source locations. For example, it provides the only information available on azimuth for the ubiquitous vertical linear array.

To determine the effect of the number of sensors  $m$  on the relative contribution of  $K$  to the Fisher information, we consider two cases. Suppose we have a regular  $d \in \{1, 2, 3\}$  dimensional array, i.e., a ULA, a regular square array, or a regular cubic array, and consider an arbitrary but fixed DOA  $\mathbf{u}$ . If the intersensor spacing is fixed so that as more sensors are added to the array its spatial extent grows, then the ratios  $J_{\phi\phi}/m$  and  $J_{\psi\psi}/m$  are proportional to  $m^{2/d} - 1$  (see Appendix A). Therefore, in this case, the directional sensitivity is only significant if  $m$  is small. On the other hand, if the array's spatial extent is fixed, i.e., the array occupies the same physical space no matter how many sensors it contains, so that as we add sensors the intersensor spacing becomes smaller, then the above ratios are proportional to  $(m^{2/d} - 1)/(m^{1/d} - 1)^2$  (see Appendix A). Thus, the relative information provided by  $K$  increases with the number of sensors. In fact, as  $m$  increases, the above ratios tend to a limit of one third of their values for the smallest  $m$  commensurate with the dimension.

Combining our observations on the directional sensitivity and the effective increase in SNR, we conclude that the vector sensors' advantage is greatest if the array is linear or planar, if it has a small number of sensors, and if the SNR is low. If the total space the array may occupy is fixed, then as the number of sensors is increased, the larger value of  $r_{\text{SNR}}$  is partly offset

by a relatively greater effect of directionality. Obviously, the smaller  $\eta$  is, the greater the advantage in using vector sensors.

#### IV. BEAMFORMING AND CAPON ESTIMATION

The CRB is a local bound related to the expected curvature of the log likelihood function. As such, it can only give local information on performance and will not reveal situations in which wide angle or ambiguity errors may occur. To examine such cases, we consider the very common beamforming and Capon direction estimators. These methods involve searching over all possible DOA's  $\Theta = [-\pi, \pi] \times [-\pi/2, \pi/2]$  for maxima of a spatial spectrum that is a measure of the power radiating from each direction  $\theta = [\phi, \psi]^T$  [22]. The beamforming and Capon spectra are

$$f_B(\theta) = \mathbf{a}^H(\theta) R \mathbf{a}(\theta) \quad (15)$$

$$f_C(\theta) = [\mathbf{a}^H(\theta) R^{-1} \mathbf{a}(\theta)]^{-1} \quad (16)$$

respectively, where  $R$  is the data covariance matrix, and  $\mathbf{a}(\theta)$  is the steering vector. Traditionally, the steering vector and covariance matrix are those of a pressure-sensor array. However, these techniques are simply adapted to the vector-sensor array by using its steering vector and covariance matrix. In practice,  $R$  must be estimated from the data, but asymptotically, (15) and (16) are obtained.

We consider a vector-sensor array's beamforming spectrum in some detail for the single source scenario. The same analysis and conclusions will apply to the Capon estimator; therefore, we do not consider it separately. When there is a single source from direction  $\theta_0$ , the beamforming spectra for pressure-sensor and vector-sensor arrays, normalized such that the maximum is unity, are

$$f_{B,P}(\theta) = \frac{\rho |\mathbf{a}_P^H(\theta) \mathbf{a}_P(\theta_0)|^2 + m}{m(m\rho + 1)} \quad (17)$$

$$f_{B,V}(\theta) = \frac{\rho(1 + \cos \gamma)^2 |\mathbf{a}_P^H(\theta) \mathbf{a}_P(\theta_0)|^2 + m(\eta + 1)}{m(4m\rho + \eta + 1)} \quad (18)$$

respectively, where  $\gamma$  is the angle between the source bearing  $\mathbf{u}_0$  and the direction of look  $\mathbf{u}$ . Under the statistical assumptions of Section II-B, the value of  $\theta$  corresponding to the maximum of  $f_{B,P}(\theta)$  is the maximum likelihood estimate. The same is true of the vector-sensor array expression only when  $\eta = 1$ , although if  $\eta$  were known, we could use  $\mathbf{a}(\theta) = \mathbf{a}_P(\theta) \otimes [\eta, \mathbf{u}^T]^T$  in (15) to obtain the maximum likelihood estimate.

It is not difficult to show that  $f_{B,V}(\theta) \leq f_{B,P}(\theta)$  for all  $\theta \in \Theta$  (as long as  $\eta \leq 3$ ), with equality holding if and only if  $\theta = \theta_0$ . Therefore, the vector-sensor array's spectrum has a sharper peak and uniformly lower sidelobes than that of the pressure-sensor array, leading to better resolution and smaller estimation errors. As in the CRB analysis, we discern, in (18), the separate effects of the increased effective SNR, which produces the  $\eta+1$  terms, and the directional sensitivity, which results in the term  $(1 + \cos \gamma)^2$ .

Of course, the larger effective SNR results in a lower background level than in the pressure-sensor array spectrum; however, it is the  $(1 + \cos \gamma)^2$  term that produces interesting results. This term further reduces the vector-sensor spectrum

relative to the pressure-sensor spectrum, the effect being greater the larger the separation between the direction of look and the true bearing. This implies two things. First, the effect of spectral leakage, i.e., the spreading of the beampattern from the invisible region to the visible [23], which occurs for any separation greater than a quarter wavelength, is considerably reduced. Second, the probability of a large ambiguity error, which occurs when noise causes the global maximum to be attained at a sidelobe, is also reduced. Therefore, the SNR (equivalently, the number of snapshots) required to reach the so-called threshold, where ambiguity errors become negligible and the CRB becomes a good measure of performance, is also reduced.

Another very important consequence of the term  $(1 + \cos \gamma)^2$  is that  $f_{B,V}(\theta) \leq f_{B,V}(\theta_0)$  with equality holding iff  $\theta = \theta_0$ . This is true for *any* array geometry. Thus, for a single source, the spectrum always has a unique global maximum corresponding to the true DOA. As a result, any vector-sensor array, linear, planar, or even a single sensor, is able to unambiguously determine both the azimuth and elevation. Indeed, [5] showed that a single vector sensor can resolve up to two sources. This means that the simple ULA, which is easy to deploy and for which fast, efficient estimation procedures exist, can be used to determine the complete DOA. This compares very favorably to the pressure-sensor ULA, which can only estimate conic angle. This is a great practical advantage. For example, when a traditional towed array, which, for obvious practical reasons, is always linear, is used to locate surface vessels, a left/right ambiguity arises, i.e., it is not known from which side of the array the signal is coming. This is resolved by rotating the vessel through  $90^\circ$  and taking another reading. However, this takes considerable time not only to turn the vessel but to wait for the array to resettle, during which period the target may have moved considerably. If a vector-sensor towed array is used, the ability to estimate the both azimuth and elevation removes the left/right ambiguity and, hence, avoids the need to rotate the vessel.

A final result of the directional sensitivity, in particular the uniqueness of the global maximum, is the suppression of grating lobes. If sensors in an array are placed more than half a wavelength apart, grating lobes, which are peaks that do not correspond to actual sources, appear in the spectra. For the pressure-sensor array, they are the same height as the mainlobe and cause irresolvable ambiguities. However, for the vector-sensor array, their height will be reduced relative to the mainlobe as a result of the directional term  $(1 + \cos \gamma)^2$ , thereby allowing the DOA to be unambiguously determined. The most well-known example of this is the pressure-sensor ULA with the usual half-wavelength spacing, which (as well as being unable to determine azimuth) is unable to distinguish between the two endfire directions. Although this ambiguity may be overcome by shifting one of the sensors so that it is less than half a wavelength from its neighbor, the reduction in the height of the grating lobe is only slight, and performance close to endfire remains poor. In addition, the computational advantages of the regular structure are lost. However, with a vector-sensor array, not only can we determine the complete bearing, but the grating lobe is suppressed down to the

background level of the spectrum. As well as allowing us to determine from which end an endfire source is coming, this also greatly improves the ability to accurately resolve sources close to endfire since the probability of making an estimate coming from the wrong end will be very small. This property allows us to use larger apertures by *deliberately* undersampling the wavefield (see [9] for an algorithm that does just this), further reducing the CRB. As we increase the spacing beyond half a wavelength, however, the grating lobe moves closer to the mainlobe, and the  $(1 + \cos \gamma)^2$  term is no longer able to completely suppress it. The result is that the threshold SNR, which is the point at which large errors can occur, increases, setting a limit on how much we may lengthen the aperture. This breakdown phenomenon was observed numerically and briefly discussed in [9] as the array aperture was increased while the SNR was held fixed. It would be very instructive to analytically examine the tradeoff between reduced CRB and increased threshold as the aperture is increased; however, we shall not do so here.

#### A. MSE Approximations

In this section, we derive closed-form expressions for the large sample mean-squared error of the beamforming and Capon estimators in the presence of multiple sources. The expressions hold equally well for vector-sensor or pressure-sensor arrays, provided the appropriate steering vector and data covariance matrix are used, and for an arbitrary number of sources  $n$ . They require that a distinct peak corresponds to each source in the asymptotic spectrum (15) or (16), i.e., all sources can be resolved asymptotically, and that the number of snapshots is large enough for the probability of nonresolution or ambiguity errors to be negligible. These extend the results of [24] and [25] by using a DOA parameterized by more than one variable, considering the beamforming estimator, and using vector-sensor arrays.

The DOA estimates provided by finding the values of  $\theta$  corresponding to the  $n$  largest maxima of (15) or (16), which are denoted  $\{\bar{\theta}_k\}_{k=1}^n$ , are known as the asymptotic DOA estimates since they require the data covariance matrix  $R$  to be known. When there is more than one source,  $\{\bar{\theta}_k\}_{k=1}^n$  are not generally equal to the true DOA's  $\{\theta_k\}_{k=1}^n$ . Using a first-order Taylor series expansion around the true DOA, the *asymptotic bias* of the  $k$ th source  $\Delta\theta_k = \bar{\theta}_k - \theta_k$  may be approximated by (see Appendix B)

$$\Delta\theta_k \approx -[\text{Re}\{D^H(\theta_k)RD(\theta_k) + H(\theta_k)\}]^{-1} \cdot \text{Re}\{D^H(\theta_k)Ra(\theta_k)\} \quad (19)$$

where

$$D(\theta) = \left[ \frac{\partial \mathbf{a}(\theta)}{\partial \phi}, \frac{\partial \mathbf{a}(\theta)}{\partial \psi} \right] \quad (20)$$

$$H(\theta) = \begin{bmatrix} \mathbf{a}^H(\theta)R \frac{\partial^2 \mathbf{a}(\theta)}{\partial \phi^2} & \mathbf{a}^H(\theta)R \frac{\partial^2 \mathbf{a}(\theta)}{\partial \phi \partial \psi} \\ \mathbf{a}^H(\theta)R \frac{\partial^2 \mathbf{a}(\theta)}{\partial \phi \partial \psi} & \mathbf{a}^H(\theta)R \frac{\partial^2 \mathbf{a}(\theta)}{\partial \psi^2} \end{bmatrix}. \quad (21)$$

The above expressions apply to the beamforming estimate to obtain the Capon estimator expression, replacing  $R$  everywhere above with  $R^{-1}$ .

When the data covariance is unknown, an estimate of the beamforming or Capon spectrum is made by using the sample covariance  $\hat{R}$  in place of  $R$  in (15) or (16). The finite sample DOA estimates, which are denoted  $\{\hat{\theta}_k\}_{k=1}^n$ , are provided by finding the  $n$  largest maxima of the estimated spectrum. As the number of snapshots becomes very large, the finite sample estimates tend to the asymptotic estimates  $\{\bar{\theta}_k\}_{k=1}^n$  with probability one. The finite sample estimates are stochastic and, thus, exhibit variability about  $\{\bar{\theta}_k\}_{k=1}^n$ . Furthermore, they need not have means equal to the asymptotic estimates. The mean square error matrix of the  $k$ th finite sample estimate  $\text{MSE}(\hat{\theta}_k)$  may be written

$$E(\hat{\theta}_k - \theta_k)(\hat{\theta}_k - \theta_k)^T = E\Delta\bar{\theta}_k\Delta\bar{\theta}_k^T + \Delta\theta_k E\Delta\bar{\theta}_k^T + E\Delta\bar{\theta}_k\Delta\theta_k^T + \Delta\theta_k\Delta\theta_k^T \quad (22)$$

where  $\Delta\bar{\theta}_k = \hat{\theta}_k - \bar{\theta}_k$  is the additional finite sample error. When  $N$  is large enough to make the probability of ambiguity errors negligible, we can approximate the additional bias  $E\Delta\bar{\theta}_k$  and variability  $E\Delta\bar{\theta}_k\Delta\bar{\theta}_k^T$  using a Taylor Series expansion of the estimated spectrum around the asymptotic estimate  $\bar{\theta}_k$  and the true data covariance matrix  $R$ . To a first-order approximation, the additional bias  $E\Delta\bar{\theta}_k$  for both estimators is zero (see Appendix B), although [25] showed that the additional bias of the Capon estimator is nonzero to second order, and it would be a simple matter to extend these results to second order. Thus

$$E(\hat{\theta}_k - \theta_k)(\hat{\theta}_k - \theta_k)^T \approx E\Delta\bar{\theta}_k\Delta\bar{\theta}_k^T + \Delta\theta_k\Delta\theta_k^T. \quad (23)$$

The first-order approximation of  $E\Delta\bar{\theta}_k\Delta\bar{\theta}_k^T$  is (see Appendix B)

$$E\Delta\bar{\theta}_k\Delta\bar{\theta}_k^T \approx \frac{1}{2N} [F(\bar{\theta}_k)]^{-1} G(\bar{\theta}_k) [F(\bar{\theta}_k)]^{-T} \quad (24)$$

where

$$\begin{aligned} F(\bar{\theta}) &= \text{Re}\{D^H(\bar{\theta})RD(\bar{\theta}) + H(\bar{\theta})\} \\ G(\bar{\theta}) &= \text{Re}\{\mathbf{a}^H(\bar{\theta})Ra(\bar{\theta})D^H(\bar{\theta})RD(\bar{\theta}) \\ &\quad - D^H(\bar{\theta})Ra(\bar{\theta})\mathbf{a}^H(\bar{\theta})RD(\bar{\theta})\}. \end{aligned}$$

The expression for the Capon estimator is obtained by replacing  $R$  everywhere with  $R^{-1}$  and the factor  $1/2N$  by  $N^2/(2(N - \tilde{m})((N - \tilde{m})^2 - 1))$ , where  $\tilde{m}$  is the number of elements in the observation vector ( $4m$  for the vector-sensor array).

For any given source scene, we can modify the procedure in [24], which calculated the asymptotic DOA estimates  $\{\bar{\theta}_k\}_{k=1}^n$  numerically to obtain an estimate of  $\text{MSE}(\hat{\theta}_k)$  that avoids any numerical maximization. First, use (19) to approximately determine the asymptotic estimate  $\bar{\theta}_k$  and the asymptotic bias  $\Delta\theta_k$ . Next, use this approximation of  $\bar{\theta}_k$  in (24) to estimate

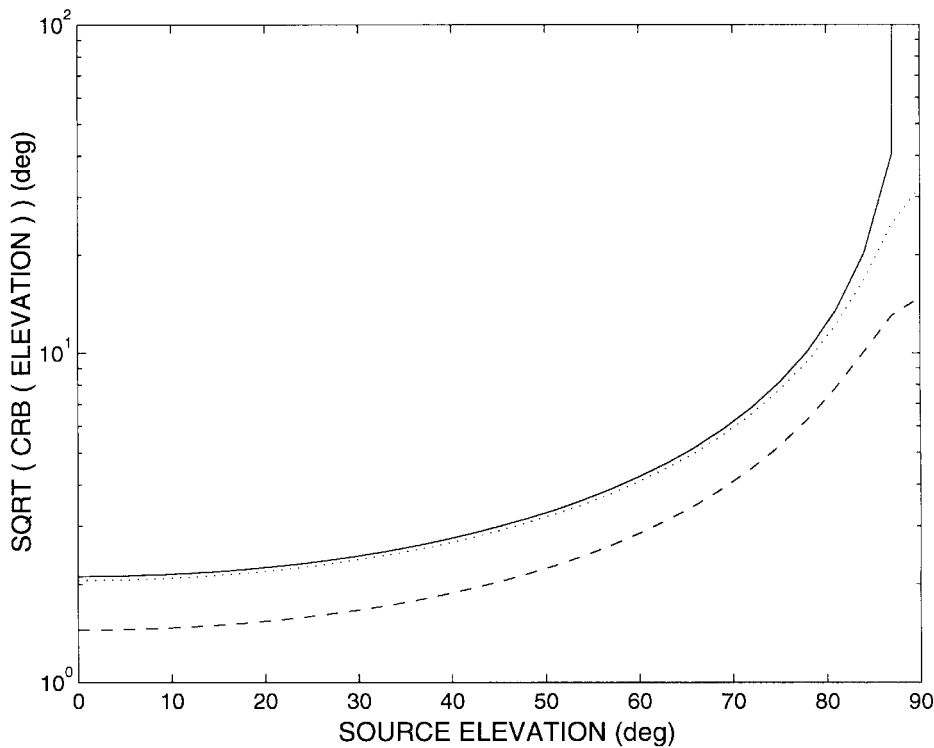


Fig. 1.  $\sqrt{\text{CRB}(\psi)}$  versus  $\psi$  (elevation) for half-wavelength spaced vector-sensor (dashed) and pressure-sensor (solid) ULA's containing eight sensors and for an undersampled vector-sensor ULA (spacing 3.5 wavelengths) containing two sensors (dotted).

the finite sample variability, and finally, combine the results in (23) to estimate the MSE.

## V. NUMERICAL EXAMPLES

In this section, we illustrate by numerical example some of the points made in Sections III and IV and verify the approximations of Section IV-A. Our attention will be restricted to the ubiquitous vertical ULA. As shown in Section IV, a pressure-sensor ULA is able to determine only elevation, whereas a vector-sensor ULA can determine the full DOA parameter vector  $\theta$ . Our comparisons will therefore consider only elevation, but it should be borne in mind that the vector-sensor ULA can also determine the azimuth. We shall use  $\eta = 1$  and a SNR  $\rho$  of zero dB.

### A. Cramér-Rao Bound

Fig. 1 shows  $\sqrt{\text{CRB}(\psi)}$  in degrees (on a logarithmic scale) plotted against the source elevation for pressure-sensor and vector-sensor arrays [for both types of array,  $\text{CRB}(\psi)$  is independent of azimuth]. The plot is for a single snapshot and should be divided by  $\sqrt{N}$  for multiple snapshots. The solid curve is for an array of eight pressure sensors with half-wavelength spacing, and the dashed curve is for an array of eight vector sensors with the same spacing. As expected, the bound is uniformly lower for the vector-sensor array than for the pressure-sensor array, and the performance of both arrays deteriorates with increasing elevation. The curves are closest at broadside, within half a degree, and diverge considerably as the source moves toward endfire (the logarithmic scale may

be deceiving). At  $\psi = 80^\circ$ , the vector-sensor curve is lower by about  $5.5^\circ$ . As the source tends to endfire, the pressure-sensor curve tends to infinity whereas the vector-sensor curve remains finite. As the source moves away from broadside, the total squared aperture seen by the oncoming wave diminishes, tending to zero at endfire. Thus, as explained in Section III-B, the inherent directional information provided by the vector sensors, which is independent of the source location, assumes a greater importance. This explains the *relative* improvement of the vector-sensor array with increasing elevation and the finiteness of the bound at endfire. For this vector-sensor array  $\sqrt{\text{CRB}(\phi)} = 14.8^\circ / (\sqrt{N} \cos \psi)$ , which is somewhat higher than the elevation bound because no phase delay information is available on azimuth.

Although the curves diverge dramatically close to endfire, this does not mean that the arrays' general performances differ as dramatically. The CRB is a strict lower bound only for unbiased estimators, and the finite range constraint on the elevation  $[-\pi/2, \pi/2]$  means that no estimator will be unbiased for all DOA's. The bias of any estimator will depend on the elevation and the number of snapshots. Generally, it will be small when  $\psi$  is far from the range constraint, i.e., near broadside, or  $N$  is large, and large when  $\psi$  is close to endfire or  $N$  is small. The result is that some estimators may actually have a lower variance than the CRB when  $\psi$  is close to endfire, and the number of snapshots is small. As  $N$  increases, however, and the bias becomes negligible, the CRB will once again lower bound the variance. Thus, when the source is close to endfire, the dramatic difference in performance suggested by these curves will only be apparent if the number of snapshots is

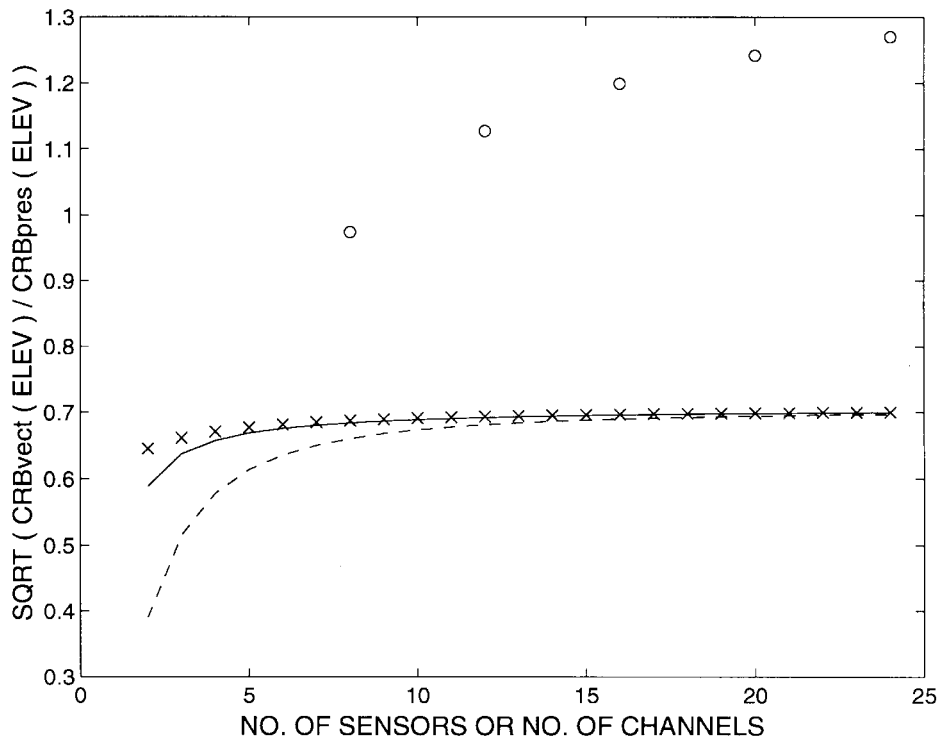


Fig. 2. Ratio of vector-sensor array bound to pressure-sensor array bound versus number of sensors. Curves are for a half-wavelength spaced vector-sensor array with  $\psi = 0^\circ$  (solid),  $70^\circ$  (dashed), and ignoring directional sensitivity ( $\times$ ) [see (12)]. Circles are for undersampled vector-sensor array with one fourth the number of sensors (i.e., same no. of channels) and occupying the same physical aperture as the pressure-sensor array. Pressure-sensor array is half-wavelength spaced for each case.

not too small. However, as discussed in Section IV the lack of endfire ambiguity does allow the vector-sensor array to provide much better estimates of sources close to endfire, but this is not apparent from the CRB.

The vector-sensor array's advantage is obtained at the expense of increased computational load: four times as many channels must be processed. It is of interest, therefore, to compare vector-sensor arrays with pressure-sensor arrays containing the same number of channels. The remaining dotted curve in Fig. 1 is for a vertical vector-sensor ULA containing two sensors and, hence, eight channels. It has the same aperture as the eight-element pressure-sensor array and, thus, an inter-sensor spacing of 3.5 wavelengths. The performance is very similar to the pressure-sensor array (solid curve), except very close to endfire. Therefore, we can estimate elevation as well as the pressure-sensor array (better near endfire), without any increase in computational load while also determining the azimuth. However, we are using a highly undersampled aperture for the vector-sensor array; thus, as discussed in Section IV, we pay for this improved performance with an increased threshold. For this array,  $\sqrt{\text{CRB}(\phi)} = 32.0^\circ / (\sqrt{N} \cos \psi)$ .

Fig. 2 shows  $\sqrt{\text{CRB}_V(\psi)/\text{CRB}_P(\psi)}$  versus number of sensors for various ULA's. All curves in the figure assume a pressure-sensor array with half-wavelength spacing, and the plotted ratio is a measure of the relative efficiency of this array to the particular vector-sensor array with which we are comparing it. The solid and dashed curves assume half-wavelength spaced vector-sensor ULA's with a vector-

sensor in the same position as each pressure sensor in the comparative array. The solid curve is for a broadside source, whereas dashed is for  $\psi = 70^\circ$ . It shows how the advantage of the vector-sensor array diminishes as the number of sensors (hence, the square projected aperture) increases, as discussed in Section III. In addition, we show (with an  $\times$ ) the value of  $\sqrt{r_{\text{SNR}}}$ , which was introduced in Section III as the above ratio after ignoring the directional sensitivity's effects. The difference between the above two curves and the curve of  $\sqrt{r_{\text{SNR}}}$  is the directional sensitivity's contribution to the bound. For the broadside source, for which the square projected aperture is largest, the directional sensitivity makes a very small contribution to the overall performance and is indistinguishable for more than about ten sensors. For the source at  $\psi = 70^\circ$ , for which the square projected aperture is much smaller, the directional sensitivity plays a far more significant role, making the vector-sensor array relatively more efficient, and only becomes indistinguishable for around 24 sensors. The limiting value of the curves, for large  $m$ , is the limiting value of  $\sqrt{r_{\text{SNR}}}$ ,  $1/\sqrt{2}$  in these examples, which depends solely on  $\eta$  (see Section III). Therefore, for large  $m$ , the directional sensitivity is irrelevant as far as elevation is concerned. Of course, it causes the bound on azimuth to decrease as  $m$  increases.

The circles in Fig. 2 exhibit undersampled ULA's containing the same number of channels as the comparative pressure-sensor array (i.e., there are four times as many pressure sensors as vector sensors) and occupying the same aperture, as described above. Again, results are for a broadside

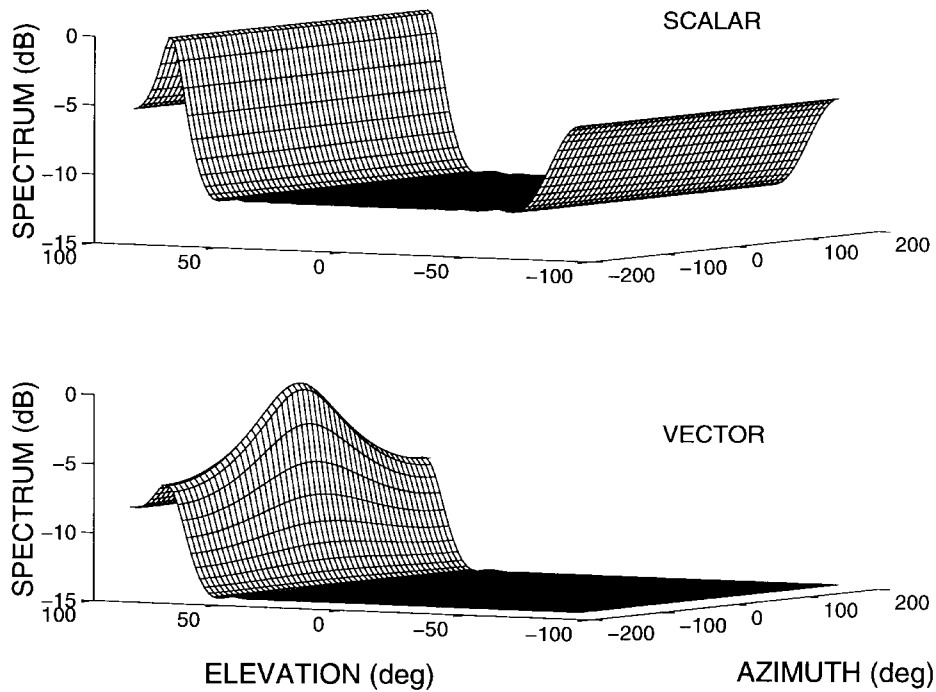


Fig. 3. Asymptotic Capon spectra for half-wavelength spaced vector-sensor and pressure-sensor ULA's with 14 sensors versus azimuth and elevation. There is a single source at  $[0^\circ, 75^\circ]$ .

source. Not surprisingly, since there is no SNR advantage due to extra measurements, the relative performance of the vector-sensor array is much worse than before. The arrays have almost equivalent performance for eight channels (two vector sensors) and the vector-sensor array's performance relatively worsens to a limit of  $\sqrt{2}$  for large  $m$ . However, as we increase  $m$ , the azimuth estimates made by the vector-sensor array improve, and the ambiguity error threshold decreases because the intersensor spacing decreases from  $3.5\lambda$  for two vector-sensors to a limit of  $2\lambda$ . It is interesting to note that for the same comparison with  $\phi = 70^\circ$ , we would obtain almost exactly the same curve. The explanation for this must be that the squared projected aperture of the undersampled vector-sensor array decreases more rapidly than that of the pressure sensor array as the source moves away from broadside, and this discrepancy is almost exactly compensated for by the relatively greater importance of the bearing-independent directional sensitivity information.

Note that it is possible to gain the benefits of the directional sensitivity of velocity sensors without the computational increase of extra channels or the increased threshold associated with the use of undersampling. An example is the diversely oriented array analyzed in [7], which consists of noncoincident single-axis velocity sensors with an equal number aligned with each axis. However, we shall not further analyze this or other possible variations here.

### B. Direction Estimation

Fig. 3 shows the asymptotic Capon spectra for half-wavelength spaced pressure-sensor and vector-sensor ULA's. Both arrays have 14 sensors, and there is a single source at  $\theta = [0^\circ, 75^\circ]^T$ . There are three points to notice. First, the

spectrum for the vector sensor array has a unique maximum instead of a line maximum indicating that azimuth is also resolvable; this is due solely to the directional sensitivity of the vector sensors. Second, the background level is 3 dB lower than in the pressure-sensor spectrum. This is due to the SNR increase and means that ambiguity errors will be negligible for a smaller number of snapshots, i.e., a reduced threshold. Last, the vector-sensor spectrum is fully suppressed at the endfire far from the source. This is the effect of the directional sensitivity and means that estimates of sources close to endfire will be much more accurate since there is no chance of making an estimate coming from the wrong end.

### C. MSE Approximation

Fig. 4 verifies the MSE approximations of Section IV by comparing an empirical MSE, which is obtained by Monte Carlo simulation using 2500 realizations, with the approximate MSE obtained by the procedure outlined in Section IV. For a single source, the MSE approximation is equal to the CRB; therefore, we consider a scenario with two 0-dB uncorrelated sources: one located at  $\theta = [-45^\circ, 20^\circ]^T$  and one at  $\theta = [35^\circ, -10^\circ]^T$ . The curves in Fig. 4 show  $\sqrt{\text{MSE}(\phi)}$ , which is the MSE for the *azimuth* of the source at  $[-45^\circ, 20^\circ]^T$ , versus number of snapshots. All curves are for a vector-sensor ULA with six sensors and half-wavelength spacing. The solid curve and the circles are the approximate and empirical MSE, respectively, of the beamforming estimate. The approximate curve tracks the empirical very closely, even for as little as 50 snapshots. The dashed curve and the stars are the approximate and empirical MSE, respectively, of the Capon estimate. The approximation tends to overestimate the true MSE, especially for small sample sizes. More snapshots are

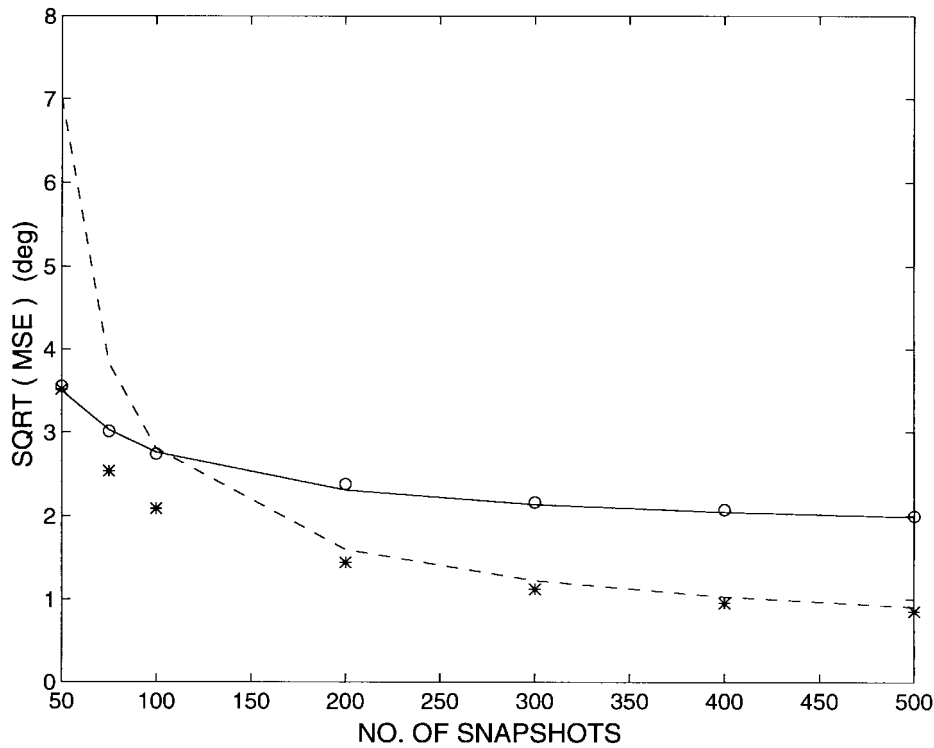


Fig. 4.  $\sqrt{\text{MSE}}$  versus number of snapshots for beamforming and Capon estimators with half-wavelength spaced ULA containing six vector sensors. There are two uncorrelated sources at  $[-45^\circ, 20^\circ]$  and  $[35^\circ, -10^\circ]$ . The approximate (solid) and empirical (o) MSE of the beamforming estimate and the approximate (dashed) and empirical (\*) MSE of the Capon estimate are shown. Results are for *azimuth* of first source.

required for an accurate approximation of the Capon MSE than the beamforming MSE, presumably because the neglected higher order terms of the Capon approximation are more significant than those of the beamforming due to the presence of a matrix inverse. Although the empirical MSE's of both estimators increase as the number of snapshots becomes small, the Capon MSE increases faster. Again, this is due to the requirement to invert the data covariance matrix for the latter estimate.

## VI. CONCLUSION

We examined the concept of using arrays of acoustic vector sensors that measure the acoustic pressure and each component of the acoustic particle velocity (introduced in [1], [2]) in some detail. We considered the CRB for a single source and ascertained two distinct improvements over the traditional pressure-sensor array: a greater number of measurements of the phase differences between noncoincident sensors, which causes an effective increase in SNR, and the inherent directional sensitivity of the vector sensors, which allows direct measurement of the DOA information available in the structure of the velocity field. By examining the CRB expressions in some detail, we showed that the directional sensitivity is most significant for linear or planar arrays (e.g., a vertical linear array where it permits estimation of azimuth) and, more generally, whenever the squared projected apertures (defined in Section III-B) are not much greater than the number of sensors. We found that as the number of sensors is increased, the relative effect of the directional sensitivity decreases if the array's aperture can grow without bound but increases if

the sensors are confined within a fixed region. Similarly, we showed that while the SNR increase is always significant, it is most effective at reducing the CRB relative to a pressure-sensor array for small numbers of sensors and low SNR's. We thus obtained the practically significant conclusion that the use of vector sensors is most advantageous when the array is required to be one or two dimensional or to possess few sensors and operate at a low SNR. This is particularly pleasing given the trend to low in-water costs that mandates smaller arrays and low SNR's.

We then extended conventional and minimum-variance beamforming methods for DOA estimation to vector-sensor arrays. Consideration of the asymptotic spectra for a single source again showed the separate effects of directional sensitivity and extra measurements. The extra measurements help to reduce the background level, therefore lowering the ambiguity threshold. The directional sensitivity, however, ensures that there is always a unique maximum. This means that any vector-sensor array can always determine both azimuth and elevation and that ambiguities (grating lobes) are not present when the wavefield is spatially undersampled. In particular, for uniform linear arrays, it resolves the endfire ambiguity and allows very accurate estimates of sources close to endfire. It also opens up the possibility of using deliberately undersampled vector-sensor arrays with a uniform spatial structure. This permits the use of an extended aperture (i.e., one larger than that obtained with standard half-wavelength spacing), so reducing the CRB while retaining the ability to use fast algorithms that exploit the regular spatial sampling as in [9]. Finally, we derived a procedure to estimate the MSE

of both azimuth and elevation for both estimators. Numerical examples were given to illustrate our conclusions and to verify the MSE approximations.

The use of vector sensors (not just acoustic [26]) is a new and emerging idea. Much work remains to be done to assess the advantages of using such sensors, but a recurring theme is the gain due to measuring a complete vector physical quantity. This need not even be done at a single location; for example, [7] analyzes a distributed component array consisting of spatially separated velocity sensors with orthogonal orientations. Furthermore, the use of nontraditional sensor types can be very fruitful; for example, [27] uses velocity sensors for hull-mounted arrays at low frequency where pressure sensors are useless. Future work should include an examination of the capability of a vector-sensor array to resolve closely spaced sources. In addition, the ability to use undersampled arrays seems to open up many exciting possibilities. An important issue, however, is the tradeoff between smaller CRB and increased threshold as the aperture is increased. An analytical study of this problem would be very useful.

#### APPENDIX A

Consider a regular  $d \in \{1, 2, 3\}$ -dimensional array that has sensors located on the vertices of a regular  $d$ -dimensional lattice with  $k$  equispaced points in each dimension. Thus, there are a total of  $m = k^d$  sensors. To comply with our assumptions in obtaining the CRB, we assume that origin is located at the array's centroid. Furthermore, to confirm to our coordinate system, consider the linear array located along the  $z$ -axis, the planar array lying in the  $x, y$ -plane, and the faces of the cubical array being orthogonal to the three axes. Consider  $J_{\phi\phi}$  and  $J_{\psi\psi}$  defined in (13) and (14), respectively. Substituting for  $\mathbf{v}_\phi$  and  $\mathbf{v}_\psi$  in these definitions, we get

$$J_{\phi\phi} = \sum_{j=1}^m (r_{jy} \cos \phi - r_{jx} \sin \phi)^2 \quad (25)$$

$$J_{\psi\psi} = \sum_{j=1}^m (r_{jz} \cos \psi - (r_{jx} \cos \phi + r_{jy} \sin \phi) \sin \psi)^2 \quad (26)$$

where  $r_{jx}$ ,  $r_{jy}$ , and  $r_{jz}$  are the  $x$ ,  $y$ , and  $z$  components of the  $j$ th sensor's position vector. Expanding the above sums will produce square terms such as  $\sum_j r_{jx}^2$  and cross terms such as  $\sum_j r_{jx} r_{jy}$  multiplied by trigonometric quantities. Under the above assumptions on the lattice, all the cross terms are zero. Furthermore, for the linear array, only  $\sum_j r_{jz}^2$  is nonzero, for the planar array,  $\sum_j r_{jz}^2 = 0$  and the remaining two squared terms are equal, and for the cubical array, all three squared terms are equal. Using these geometrical results in (25) and (26), we obtain

$$J_{\phi\phi} \propto \sum_{j=1}^m r_{jx}^2, \quad (27)$$

$$J_{\psi\psi} \propto \sum_{j=1}^m r_{jx}^2 \quad (28)$$

for the planar and cubical arrays. For the linear array,  $J_{\phi\phi}$  is zero, and (28) becomes  $J_{\psi\psi} \propto \sum_j r_{jz}^2$ . A similar expansion of the off-diagonal terms of the FIM for all three regular arrays shows that they are zero. Calculating the above sums for the three lattices, we obtain

$$\sum_{j=1}^m r_{jx}^2 = \begin{cases} 2k^{d-1}s^2 \sum_{l=1}^{k/2} \left(\frac{2l-1}{2}\right)^2 & k \text{ even} \\ 2k^{d-1}s^2 \sum_{l=1}^{(k-1)/2} l^2 & k \text{ odd} \end{cases} \quad (29)$$

where  $s$  is the intersensor spacing. This holds for the planar and cubical arrays, and  $\sum_j r_{jz}^2$  for the linear array is also given by the right-hand side of (29). Using the arithmetic series identity

$$\sum_{l=1}^{(k-1)/2} l^2 = \sum_{l=1}^{k/2} \left(\frac{2l-1}{2}\right)^2 = \frac{k(k^2-1)}{24}$$

it follows that  $J_{\phi\phi}/m$  and  $J_{\psi\psi}/m$  are proportional to  $s^2(k^2-1)$  for all three arrays (except that  $J_{\phi\phi} = 0$  for the linear array).

When the intersensor spacing is held fixed and the array grows without bound,  $s$  is constant. Thus,  $J_{\phi\phi}/m$  and  $J_{\psi\psi}/m$  are proportional to  $(k^2-1) = m^{2/d} - 1$ . When the spatial extent of the array is fixed, the intersensor spacing  $s$  decreases as we add more sensors. If the lattice has constant length  $c$ , say, in each dimension, then the intersensor spacing is  $s = c/(k-1)$ . Thus,  $J_{\phi\phi}/m$  and  $J_{\psi\psi}/m$  are proportional to  $(k^2-1)/(k-1)^2 = (m^{2/d} - 1)/(m^{1/d} - 1)^2$ .

#### APPENDIX B

The beamforming and Capon estimates  $\{\hat{\boldsymbol{\theta}}_k\}_{k=1}^n$  are obtained by minimizing or maximizing a function of the form

$$\hat{f}(\boldsymbol{\theta}) = \mathbf{a}^H(\boldsymbol{\theta}) \hat{K} \mathbf{a}(\boldsymbol{\theta}) \quad (30)$$

where  $\hat{K}$  is a consistent Hermitian estimate of a Hermitian matrix  $K$ . Beamforming estimates are obtained by maximizing (30) with  $K = R$  and Capon estimates by minimizing (30) with  $K = R^{-1}$ . Denote by  $f(\boldsymbol{\theta})$  the right-hand side of (30) with  $\hat{K}$  replaced by  $K$ . The asymptotic estimates  $\{\hat{\boldsymbol{\theta}}_k\}_{k=1}^n$  are then the maximizers or minimizers of  $f(\boldsymbol{\theta})$ . Using a first-order Taylor series expansion of  $\partial f(\boldsymbol{\theta})/\partial \boldsymbol{\theta}$  around  $\boldsymbol{\theta}_k$ , we have

$$\frac{\partial f(\bar{\boldsymbol{\theta}}_k)}{\partial \boldsymbol{\theta}} = \frac{\partial f(\boldsymbol{\theta}_k)}{\partial \boldsymbol{\theta}} + \frac{\partial^2 f(\boldsymbol{\theta}_k)}{\partial \boldsymbol{\theta} \partial \boldsymbol{\theta}^T} \Delta \boldsymbol{\theta}_k + O(|\Delta \boldsymbol{\theta}_k|^2) = 0.$$

Rearranging gives the asymptotic bias as

$$\Delta \boldsymbol{\theta}_k \triangleq \bar{\boldsymbol{\theta}}_k - \boldsymbol{\theta}_k = - \left[ \frac{\partial^2 f(\boldsymbol{\theta}_k)}{\partial \boldsymbol{\theta} \partial \boldsymbol{\theta}^T} \right]^{-1} \frac{\partial f(\boldsymbol{\theta}_k)}{\partial \boldsymbol{\theta}} + O(|\Delta \boldsymbol{\theta}_k|^2).$$

Differentiating (30) with respect to  $\boldsymbol{\theta}$  gives

$$\frac{\partial f(\boldsymbol{\theta}_k)}{\partial \boldsymbol{\theta}} = 2 \operatorname{Re}[D^H(\boldsymbol{\theta}_k) K \mathbf{a}(\boldsymbol{\theta}_k)] \quad (31)$$

$$\frac{\partial^2 f(\boldsymbol{\theta}_k)}{\partial \boldsymbol{\theta} \partial \boldsymbol{\theta}^T} = 2 \operatorname{Re}[D^H(\boldsymbol{\theta}_k) K D(\boldsymbol{\theta}_k) + H(\boldsymbol{\theta}_k)] \quad (32)$$

where  $D(\cdot)$  and  $H(\cdot)$  are defined in (20) and (21), respectively. Thus, we get

$$\Delta\boldsymbol{\theta}_k = -[\text{Re}[D^H(\boldsymbol{\theta}_k)KD(\boldsymbol{\theta}_k) + H(\boldsymbol{\theta}_k)]]^{-1} \cdot \text{Re}[D^H(\boldsymbol{\theta}_k)K\mathbf{a}(\boldsymbol{\theta}_k)] + O(|\Delta\boldsymbol{\theta}_k|^2).$$

Replacing  $K$  by  $R$  or  $R^{-1}$ , as appropriate, gives (19).

To obtain the additional finite sample bias  $E\Delta\bar{\boldsymbol{\theta}}_k = E\hat{\boldsymbol{\theta}}_k - \bar{\boldsymbol{\theta}}_k$ , we parallel the development of [25]. Now, consider  $g(\boldsymbol{\theta}, K) = f(\boldsymbol{\theta})$  as a function of both  $\boldsymbol{\theta}$  and  $K$  and make a first-order expansion of its derivative with respect to  $\boldsymbol{\theta}$  about  $(\bar{\boldsymbol{\theta}}, K)$

$$\begin{aligned} \frac{\partial g(\hat{\boldsymbol{\theta}}_k, \hat{K})}{\partial \boldsymbol{\theta}} &= \frac{\partial g(\bar{\boldsymbol{\theta}}_k, K)}{\partial \boldsymbol{\theta}} + \frac{\partial^2 g(\bar{\boldsymbol{\theta}}_k, K)}{\partial \boldsymbol{\theta} \partial \boldsymbol{\theta}^T} \Delta\bar{\boldsymbol{\theta}}_k \\ &+ \text{Tr} \left\{ \left[ \frac{\partial}{\partial K} \frac{\partial g(\bar{\boldsymbol{\theta}}_k, K)}{\partial \boldsymbol{\theta}} \right]^T \Delta K \right\} \\ &+ O(|\Delta\bar{\boldsymbol{\theta}}_k|^2, \|\Delta K\|^2) = 0 \end{aligned} \quad (33)$$

where  $\Delta K = \hat{K} - K$ . Similarly to [25, Appendix B]

$$\text{Tr} \left\{ \left[ \frac{\partial}{\partial K} \frac{\partial g(\bar{\boldsymbol{\theta}}_k, K)}{\partial \boldsymbol{\theta}} \right]^T \Delta K \right\} = 2 \text{Re}(D^H(\bar{\boldsymbol{\theta}}_k) \Delta K \mathbf{a}(\bar{\boldsymbol{\theta}}_k)) \quad (34)$$

which requires only that  $\Delta K$  is Hermitian. Since  $\bar{\boldsymbol{\theta}}_k$  is the asymptotic estimate, the first term on the right-hand side of (33) is zero. Furthermore,  $g(\bar{\boldsymbol{\theta}}_k, K) = f(\bar{\boldsymbol{\theta}}_k)$ . Therefore, from (32)–(34), we have the additional bias

$$\begin{aligned} E\Delta\bar{\boldsymbol{\theta}}_k &= -\{\text{Re}[D^H(\bar{\boldsymbol{\theta}}_k)KD(\bar{\boldsymbol{\theta}}_k) + H(\bar{\boldsymbol{\theta}})]\}^{-1} \\ &\cdot \text{Re}[D^H(\bar{\boldsymbol{\theta}}_k)E\Delta K\mathbf{a}(\bar{\boldsymbol{\theta}}_k)] \\ &+ O(|\Delta\bar{\boldsymbol{\theta}}_k|^2, E\|\Delta K\|^2). \end{aligned} \quad (35)$$

Since  $E\Delta R = E\hat{R} - R = 0$ , the additional bias is clearly zero for the beamforming estimator. We are using the usual estimate for  $R^{-1}$ , i.e., the inverse of the maximum likelihood estimate of  $R$ , which is biased. To be precise,  $E\hat{R}^{-1} = R^{-1}N/(N - \tilde{m})$  [28], where  $\tilde{m}$  is number of elements in the observation vector ( $4m$  for the vector-sensor array and  $m$  for the pressure-sensor array). Note this is the estimate used in [24]; however, in that paper, the additional bias was not considered. On the other hand, [25] considered the less commonly used unbiased estimate of  $R^{-1}$ , leading immediately to zero additional bias. Hence, from (35), we get

$$\begin{aligned} E\Delta\bar{\boldsymbol{\theta}}_k &= -\frac{\tilde{m}}{N - \tilde{m}} \{\text{Re}[D^H(\bar{\boldsymbol{\theta}}_k)R^{-1}D(\bar{\boldsymbol{\theta}}_k) + H(\bar{\boldsymbol{\theta}})]\}^{-1} \\ &\cdot \text{Re}[D^H(\bar{\boldsymbol{\theta}}_k)R^{-1}\mathbf{a}(\bar{\boldsymbol{\theta}}_k)] = 0. \end{aligned}$$

The final equality follows from (31) and the fact that  $\bar{\boldsymbol{\theta}}_k$  is a minimizer of  $f(\boldsymbol{\theta})$ , again giving zero additional bias to first order.

Since the additional bias of both estimates is zero, the MSE is given by (23). To determine the variability of the finite

sample estimate, consider that from (33) and (34), we have

$$\begin{aligned} \Delta\bar{\boldsymbol{\theta}}_k \Delta\bar{\boldsymbol{\theta}}_k^T &= 4 \left[ \frac{\partial^2 f(\bar{\boldsymbol{\theta}}_k)}{\partial \boldsymbol{\theta} \partial \boldsymbol{\theta}^T} \right]^{-1} \text{Re}[D^H(\bar{\boldsymbol{\theta}}_k) \Delta K \mathbf{a}(\bar{\boldsymbol{\theta}}_k)] \\ &\cdot \text{Re}[D^H(\bar{\boldsymbol{\theta}}_k) \Delta K \mathbf{a}(\bar{\boldsymbol{\theta}}_k)]^T \left[ \frac{\partial^2 f(\bar{\boldsymbol{\theta}}_k)}{\partial \boldsymbol{\theta} \partial \boldsymbol{\theta}^T} \right]^{-T} \\ &+ O(|\Delta\bar{\boldsymbol{\theta}}_k|^4, \|\Delta K\|^4). \end{aligned}$$

Since  $\hat{\boldsymbol{\theta}}_k$  and  $\hat{K}$  are consistent, we ignore the  $O$  term. We shall also drop the dependence on  $\bar{\boldsymbol{\theta}}_k$  for clarity of exposition. Using the fact that for an arbitrary complex vector  $\mathbf{u}$

$$\text{Re}(\mathbf{u}) \text{Re}(\mathbf{u}^T) = \text{Re}(\mathbf{u}\mathbf{u}^H + \mathbf{u}\mathbf{u}^T)/2$$

we can write

$$\begin{aligned} \Delta\bar{\boldsymbol{\theta}}_k \Delta\bar{\boldsymbol{\theta}}_k^T &= 2 \left[ \frac{\partial^2 f(\bar{\boldsymbol{\theta}}_k)}{\partial \boldsymbol{\theta} \partial \boldsymbol{\theta}^T} \right]^{-1} \text{Re}[D^H \Delta K \mathbf{a} \mathbf{a}^H \Delta K D] \\ &+ D^H \Delta K \mathbf{a} \mathbf{a}^T \Delta K^* D^* \left[ \frac{\partial^2 f(\bar{\boldsymbol{\theta}}_k)}{\partial \boldsymbol{\theta} \partial \boldsymbol{\theta}^T} \right]^{-T} \end{aligned}$$

where the superscript  $*$  indicates complex conjugation without transposition. Expanding  $\Delta K$ , taking expectations, and regrouping, we get

$$\begin{aligned} E\Delta\bar{\boldsymbol{\theta}}_k \Delta\bar{\boldsymbol{\theta}}_k^T &= 2 \left[ \frac{\partial^2 f(\bar{\boldsymbol{\theta}}_k)}{\partial \boldsymbol{\theta} \partial \boldsymbol{\theta}^T} \right]^{-1} \text{Re}[D^H K \mathbf{a} (\mathbf{a}^H K D + \mathbf{a}^T K^* D^*) \\ &- D^H K \mathbf{a} (\mathbf{a}^H E \hat{K} D + \mathbf{a}^T E \hat{K}^* D^*) \\ &- D^H E \hat{K} \mathbf{a} (\mathbf{a}^H K D + \mathbf{a}^T K^* D^*) \\ &+ E\{D^H \hat{K} \mathbf{a} (\mathbf{a}^H \hat{K} D + \mathbf{a}^T \hat{K}^* D^*)\}] \\ &\cdot \left[ \frac{\partial^2 f(\bar{\boldsymbol{\theta}}_k)}{\partial \boldsymbol{\theta} \partial \boldsymbol{\theta}^T} \right]^{-T}. \end{aligned} \quad (36)$$

Now, consider the first term in the summation

$$\begin{aligned} \text{Re}[D^H K \mathbf{a} (\mathbf{a}^H K D + \mathbf{a}^T K^* D^*)] \\ = 2 \text{Re}[D^H K \mathbf{a}] \text{Re}[\mathbf{a}^H K D]^T = 0. \end{aligned} \quad (37)$$

The last equality follows from (31) and the fact that  $\bar{\boldsymbol{\theta}}_k$  is a minimum or maximum of  $f(\boldsymbol{\theta})$ . Similarly, for the second and third terms in the summation of (36)

$$\begin{aligned} \text{Re}[D^H K \mathbf{a} (\mathbf{a}^H E \hat{K} D + \mathbf{a}^T E \hat{K}^* D^*)] \\ = 2 \text{Re}[D^H K \mathbf{a}] \text{Re}[D^H E \hat{K} \mathbf{a}]^T = 0 \\ \text{Re}[D^H E \hat{K} \mathbf{a} (\mathbf{a}^H K D + \mathbf{a}^T K^* D^*)] \\ = 2 \text{Re}[D^H E \hat{K} \mathbf{a}] \text{Re}[D^H K \mathbf{a}]^T = 0. \end{aligned}$$

This leaves

$$\begin{aligned} E\Delta\bar{\boldsymbol{\theta}}_k \Delta\bar{\boldsymbol{\theta}}_k^T &= 4 \left[ \frac{\partial^2 f(\bar{\boldsymbol{\theta}}_k)}{\partial \boldsymbol{\theta} \partial \boldsymbol{\theta}^T} \right]^{-1} E\{\text{Re}[D^H \hat{K} \mathbf{a}] \text{Re}[D^H \hat{K} \mathbf{a}]^T\} \\ &\cdot \left[ \frac{\partial^2 f(\bar{\boldsymbol{\theta}}_k)}{\partial \boldsymbol{\theta} \partial \boldsymbol{\theta}^T} \right]^{-T} \end{aligned} \quad (38)$$

which of course tends to zero as  $\hat{K} \rightarrow K$ . Only the middle term of this expression remains to be calculated; the factors

on either end are given by (32) with  $R$  or  $R^{-1}$  substituted for  $K$ , as appropriate.

Consider the covariance of  $\hat{R}$ , which is given by  $\text{Cov}(\hat{R}_{ij}, \hat{R}_{kl}) = R_{ik}R_{lj}/N$  [28]. Thus

$$\begin{aligned} E\hat{R}_{ij}\hat{R}_{kl} &= \frac{1}{N} R_{il}R_{kj} + R_{ij}R_{kl}, \\ E\hat{R}_{ij}\hat{R}_{kl}^* &= \frac{1}{N} R_{ik}R_{lj} + R_{ij}R_{lk}. \end{aligned}$$

Using these, we can calculate the  $(m, n)$ th entry of the middle term of (38). Again, dropping the dependence on  $\bar{\theta}_k$  for clarity and letting  $\mathbf{d}_i$  denote the  $i$ th column of  $D$

$$\begin{aligned} E\{\text{Re}[D^H \hat{K} \mathbf{a}] \text{Re}[D^H \hat{K} \mathbf{a}]^T\}_{mn} \\ = \frac{1}{2} \{\text{Re}[E(\mathbf{d}_m^H \hat{R} \mathbf{a} \mathbf{a}^H \hat{R} \mathbf{d}_n + \mathbf{d}_m^H \hat{R} \mathbf{a} \mathbf{a}^T \hat{R}^* \mathbf{d}_n^*)]\} \end{aligned} \quad (39)$$

$$\begin{aligned} = \frac{1}{2N} \{\text{Re}[\mathbf{a}^H R \mathbf{d}_n \mathbf{d}_n^H R \mathbf{a} + \mathbf{d}_m^H R \mathbf{a} \mathbf{d}_n^H R \mathbf{a} \\ + N(\mathbf{d}_m^H R \mathbf{a} \mathbf{a}^H R \mathbf{d}_n + \mathbf{d}_m^H R \mathbf{a} \mathbf{d}_n^H R \mathbf{a})]\}. \end{aligned} \quad (40)$$

Similarly to (37), the real part of the sum of the last two terms is zero. For the same reason,  $\mathbf{d}_i R \mathbf{a}$  is purely imaginary for any  $i$ ; therefore

$$\text{Re}[\mathbf{d}_m^H R \mathbf{a} \mathbf{d}_n^H R \mathbf{a}] = -\mathbf{d}_m^H R \mathbf{a} \mathbf{a}^H R \mathbf{d}_n. \quad (41)$$

Finally

$$\begin{aligned} E\Delta\bar{\theta}_k\Delta\bar{\theta}_k^T &= \{\text{Re}[D^H R D + H]\}^{-1} \\ &\cdot \frac{\mathbf{a}^H R \mathbf{a} \text{Re}[D^H R D] - D^H R \mathbf{a} \mathbf{a}^H R D}{2N} \\ &\cdot \{\text{Re}[D^H R D + H]\}^{-1} \end{aligned}$$

where all quantities are calculated at  $\bar{\theta}_k$

For the Capon estimator, from [28], we can obtain

$$\begin{aligned} E\hat{R}_{ij}^{-1}\hat{R}_{kl}^{-1} &= \frac{N^2}{(N - \tilde{m} + 1)(N - \tilde{m} - 1)} \\ &\cdot \left\{ \frac{R_{il}^{-1}R_{kj}^{-1}}{N - \tilde{m}} + R_{ij}^{-1}R_{kl}^{-1} \right\} \\ E\hat{R}_{ij}^{-1}(\hat{R}_{kl}^{-1})^* &= \frac{N^2}{(N - \tilde{m} + 1)(N - \tilde{m} - 1)} \\ &\cdot \left\{ \frac{R_{ik}^{-1}R_{lj}^{-1}}{N - \tilde{m}} + R_{ij}^{-1}R_{lk}^{-1} \right\}. \end{aligned}$$

Using these expressions in the arguments of (39)–(41) results in

$$\begin{aligned} E\Delta\bar{\theta}_k\Delta\bar{\theta}_k^T \\ = \{\text{Re}[D^H R^{-1} D + H]\}^{-1} \\ \cdot \frac{\mathbf{a}^H R^{-1} \mathbf{a} \text{Re}[D^H R^{-1} D] - D^H R^{-1} \mathbf{a} \mathbf{a}^H R^{-1} D}{2(N - \tilde{m})(N - \tilde{m} + 1)(N - \tilde{m} - 1)/N^2} \\ \cdot \{\text{Re}[D^H R^{-1} D + H]\}^{-1} \end{aligned}$$

where all quantities are calculated at  $\bar{\theta}_k$ .

## REFERENCES

- [1] A. Nehorai and E. Paldi, "Acoustic vector-sensor array processing," in *Proc. 26th Asilomar Conf. Signals, Syst., Comput.*, Pacific Grove, CA, Oct. 1992, pp. 192–198.
- [2] ———, "Acoustic vector-sensor array processing," *IEEE Trans. Signal Processing*, vol. 42, pp. 2481–2491, Sept. 1994.
- [3] M. J. Berliner and J. F. Lindberg, Eds., *Acoustic Particle Velocity Sensors: Design, Performance and Applications*. Woodbury, NY: AIP, 1996.
- [4] J. C. Nickles *et al.*, "A vertical array of directional acoustic sensors," in *Proc. Mast. Oceans Tech. (Oceans'92)*, Newport, RI, Oct. 1992, pp. 340–345.
- [5] B. Hochwald and A. Nehorai, "Identifiability in array processing models with vector-sensor applications," *IEEE Trans. Signal Processing*, vol. 44, pp. 83–95, Jan. 1996.
- [6] M. Hawkes and A. Nehorai, "Acoustic vector-sensor beamforming and Capon direction estimation," in *Proc. Int. Conf. Acoust., Speech, Signal Process. (ICASSP)*, Detroit, MI, May 1995, pp. 1673–1676.
- [7] ———, "Bearing estimation with acoustic vector-sensor arrays," presented at *Acoust. Velocity-Sensor Focused Workshop*, Mystic, CT, Sept. 1995; published in [3, pp. 345–358].
- [8] K. T. Wong and M. D. Zoltowski, "Orthogonal velocity-hydrophone ESPRIT for sonar source localization," in *Proc. MTS/IEEE Oceans Conf.*, Fort Lauderdale, FL, Sept. 1996, vol. 3, pp. 1307–1311.
- [9] ———, "ESPRIT-based extended-aperture source localization using velocity-hydrophones," in *Proc. MTS/IEEE Oceans Conf.*, Fort Lauderdale, FL, Sept. 1996, vol. 3, pp. 1427–1432.
- [10] ———, "Source localization by 2-D root-MUSIC with 'scalar triads' of velocity-hydrophones," in *Proc. 39th Midwest Symp. Circuits Syst.*, Ames, IA, Aug. 1996, pp. 677–680.
- [11] G. L. D'Spain and W. S. Hodgkiss, "The simultaneous measurement of infrasonic acoustic particle velocity and acoustic pressure in the ocean by freely drifting swallow floats," *IEEE J. Oceanic Eng.*, vol. 16, pp. 195–207, Apr. 1991.
- [12] G. L. D'Spain, W. S. Hodgkiss, and G. L. Edmonds, "Energetics of the deep ocean's infrasonic sound field," *J. Acoust. Soc. Amer.*, vol. 89, no. 3, pp. 1134–1158, Mar. 1991.
- [13] G. L. D'Spain *et al.*, "Initial analysis of the data from the vertical DIFAR array," in *Proc. Mast. Oceans Tech. (Oceans'92)*, Newport, RI, Oct. 1992, pp. 346–351.
- [14] V. A. Shchurov, V. I. Ilyichev, and V. P. Kuleshov, "The ambient noise energy motion in the near-surface layer in the ocean," *J. Physique*, vol. 4, no. 5, pt. 2, pp. 1273–1276, May 1994.
- [15] J. Capon, "High resolution frequency-wavenumber spectrum analysis," *Proc. IEEE*, vol. 57, pp. 1408–1418, Aug. 1969.
- [16] A. D. Pierce, *Acoustics: An Introduction to Its Physical Principles and Applications*. New York: McGraw-Hill, 1981.
- [17] M. Hawkes and A. Nehorai, "Effects of sensor placement on acoustic vector-sensor array performance," submitted for publication.
- [18] ———, "Acoustic vector-sensor beamforming and Capon direction estimation," Tech. Rep. UIC-EECS-96-4, Dept. Elect. Eng. Comput. Sci., Univ. Illinois at Chicago, Nov. 1996.
- [19] R. Kneipfer, "Spatial auto and cross-correlation functions for tri-axial velocity sensor outputs in a narrowband, three-dimensional, isotropic pressure field," Sept. 1995, private communication.
- [20] G. C. Lauchle, J. F. McEachern, A. R. Jones, and J. A. McConnell, "Flow-induced noise on pressure gradient hydrophones," in *Acoustic Particle Velocity Sensors: Design, Performance and Applications*. Woodbury, NY: AIP, 1996, pp. 202–225.
- [21] S. H. Ko and H. H. Schloemer, "Flow noise reduction techniques for a planar array of hydrophones," *J. Acoust. Soc. Amer.*, vol. 92, no. 9, pp. 3409–3424.
- [22] D. H. Johnson, "The application of spectral estimation methods to bearing estimation problems," *Proc. IEEE*, vol. 70, Sept. 1982.
- [23] D. H. Johnson and D. E. Dudgeon, *Array Signal Processing: Concepts and Techniques*. Englewood Cliffs, NJ: Prentice-Hall, 1993.
- [24] P. Stoica, P. Händel, and T. Söderström, "Study of Capon method for array signal processing," *Circuits Syst. Signal Process.*, vol. 14, no. 6, pp. 749–770, 1995.
- [25] C. Vaidyanathan and K. M. Buckley, "Performance analysis of the MVDR spatial spectrum estimator," *IEEE Trans. Signal Processing*, vol. 43, pp. 1427–1437, June 1995.
- [26] A. Nehorai and E. Paldi, "Vector-sensor array processing for electromagnetic source localization," *IEEE Trans. Signal Processing*, vol. 42, pp. 376–398, Feb. 1994.

- [27] M. Hawkes and A. Nehorai, "Surface-mounted acoustic vector-sensor array processing," in *Proc. Int. Conf. Acoust., Speech Signal Process. (ICASSP)*, Atlanta, GA, May 1996, pp. 3170–3173.
- [28] D. R. Brillinger, *Time Series Data Analysis and Theory*. New York: Holt, 1975.



**Malcolm Hawkes** (S'95) was born in Stockton-on-Tees, U.K., in 1970 and grew up in Swansea, U.K. He received the B.A. degree in electrical and information science from the University of Cambridge, Cambridge, U.K., in 1992, the M.Sc. degree in applied statistics from the University of Oxford, Oxford, U.K., in 1993, and the M.S. and M.Phil. degrees in electrical engineering from Yale University, New Haven, CT, in 1995 and 1998, respectively. He is currently a Visiting Scholar at the University of Illinois, Chicago, where he is

completing his thesis for the Ph.D. degree in electrical engineering from Yale University. From 1988 to 1989, and again in the Summers of 1990 and 1991, he worked at GEC-Marconi Research Centre, Chelmsford, U.K., on a variety of projects. His research interests include statistical signal processing with applications in array processing and biomedicine.

Mr. Hawkes received the John and Grace Nuveen International Scholar Award from the University of Illinois, Chicago, in 1998.



**Arye Nehorai** (S'80–M'83–SM'90–F'94) received the B.Sc. and M.Sc. degrees in electrical engineering from the Technion—Israel Institute of Technology, Haifa, in 1976 and 1979, respectively, and the Ph.D. degree in electrical engineering from Stanford University, Stanford, CA, in 1983.

After graduation, he was a Research Engineer at Systems Control Technology, Inc., Palo Alto, CA. From 1985 to 1995, he was with the Department of Electrical Engineering, Yale University, New Haven, CT, where he became an Associate Professor in 1989. In 1995, he joined the Department of Electrical Engineering and Computer Science at the University of Illinois, Chicago (UIC), as a Full Professor. He holds a joint professorship with the Bioengineering Department at UIC.

Dr. Nehorai is an Associate Editor of the IEEE TRANSACTIONS ON ANTENNAS AND PROPAGATION, the IEEE JOURNAL OF OCEANIC ENGINEERING, *Circuits, Systems, and Signal Processing*, and *The Journal of the Franklin Institute* and has been an Associate Editor of the IEEE TRANSACTIONS ON ACOUSTICS, SPEECH, AND SIGNAL PROCESSING. He served as the Chairman of the Connecticut IEEE Signal Processing Chapter from 1986 to 1995 and is currently Vice-Chair of the IEEE Signal Processing Society's Technical Committee on Sensor Array and Multichannel (SAM) Processing. He was co-recipient, with P. Stoica, of the 1989 IEEE Signal Processing Society's Senior Award for Best Paper. He has been a Fellow of the Royal Statistical Society since 1996.